

Progenitor mass and ejecta asymmetry of SN 2023ixf from nebular spectroscopy

Lucía Ferrari^{1,2} * , Gastón Folatelli^{1,2,3} , Keila Ertini^{1,2} , Hanindy Kuncarayakti^{4,5} , and Jennifer E. Andrews⁶ 

¹ Instituto de Astrofísica de La Plata, Paseo del Bosque S/N, 1900, Buenos Aires, Argentina

² Facultad de Ciencias Astronómicas y Geofísicas Universidad Nacional de La Plata, Paseo del Bosque S/N B1900FWA, La Plata, Argentina

³ Kavli Institute for the Physics and Mathematics of the Universe (WPI), The University of Tokyo, Kashiwa, 277-8583 Chiba, Japan

⁴ Finnish Centre for Astronomy with ESO (FINCA), 20014 University of Turku, Finland

⁵ Tuorla Observatory, Department of Physics and Astronomy, 20014 University of Turku, Finland

⁶ Gemini Observatory/NSF's NOIRLab, 670 N. A'ohoku Place, Hilo, HI 96720, USA

Received April 18, 2024; accepted Month XX, XXXX

ABSTRACT

Context. SN 2023ixf was discovered in galaxy M101 on May 2023. Its proximity made it an extremely valuable opportunity for the scientific community to study the characteristics of the SN and its progenitor. A point source detected on archival images and hydrodynamical modelling of the bolometric light curve has been used to constrain the former star's properties. There is a significant variation in the published results regarding the initial mass of the progenitor. Nebular spectroscopy provides an independent tool to enhance our understanding of the supernova and its progenitor.

Aims. We determine the SN progenitor mass by studying the first published nebular spectrum taken 259 days after the explosion.

Methods. We analyze the nebular spectrum taken with GMOS at the Gemini North Telescope. Typical emission lines are identified, such as [O I], H α , [Ca II], among others. Some species' line profiles show broad and narrow components, indicating two ejecta velocities and an asymmetric ejecta. We infer the progenitor mass of SN 2023ixf by comparing with synthetic spectra and by measuring the forbidden oxygen doublet flux.

Results. Based on the flux ratio and the direct comparison with spectra models, the progenitor star of SN 2023ixf had a M_{ZAMS} between 12 and 15 M_{\odot} . In comparison with this, we find the use of the [O I] doublet flux to be less constraining of the progenitor mass. Our results agree with those from hydrodynamical modelling of the early light curve and pre-explosion image estimates pointing to a relatively low-mass progenitor.

Key words. supernovae:general — supernovae: individual: SN 2023ixf

1. Introduction

One key aspect of astrophysics is understanding the fate of massive stars and the origin of supernova (SN) explosions. Hydrogen-rich SNe, known as Type II SNe (SNe II), arise from the core collapse of stars more massive than about 8 M_{\odot} during the red supergiant (RSG) phase, as has been confirmed through direct progenitor detections (Maund et al. 2005; Van Dyk et al. 2012; Smartt 2015). However, there is an apparent contradiction between theory and observations on the high-end range of SN-II progenitor masses. Direct detections appear to show a lack of progenitors more massive than 17 – 18 M_{\odot} while the theoretical limit should be around 25 – 30 M_{\odot} (Smartt 2015). Although several explanations have been proposed to explain this apparent controversy (Davies & Beasor 2018), it is of utmost importance to determine the masses of SNe-II progenitors.

Apart from direct detections on pre-explosions images, which is a powerful method albeit limited to the nearby Universe, there are other more indirect ways to derive progenitor properties. One such method is through the modelling of the nebular-phase spectra. Once the plateau phase ends, most of the SN ejecta become transparent and the spectral emission origi-

nates from regions near the former stellar core. Analysis of the nebular spectrum reveals properties of the core, such as its mass (Jerkstrand et al. 2012; Kuncarayakti et al. 2015; Dessart et al. 2021). The stellar-core mass is in turn indicative of the initial mass with which the star was formed. Furthermore, the shape of the emission lines provides information about the distribution of the innermost ejecta and thus can give hints on the possible asymmetries that may occur during the explosion (Taubenberger et al. 2009; Fang et al. 2022).

Type II SN 2023ixf, discovered in M101, was one of the most nearby SNe discovered in the last few decades. Due to its proximity, it raised the interest of professional and amateur astronomers alike. A veritable wealth of articles and communications have been issued since its discovery in May 2023. Part of these analyses focused on early-time time observations across the electromagnetic spectrum. The presence of a dense circumstellar material surrounding the SN was revealed by early-on high ionization "flash" spectral lines (Perley et al. 2023; Jacobson-Galán et al. 2023; Smith et al. 2023; Bostroem et al. 2023; Hiramatsu et al. 2023; Teja et al. 2023), along with an early excess in the light curve, especially in the ultraviolet range (Jacobson-Galán et al. 2023; Hosseinzadeh et al. 2023; Teja et al. 2023; Martínez et al. 2023), and X-ray, radio and polarimetry

* luciaferrari@fcaglp.unlp.edu.ar

observations (Grefenstette et al. 2023; Berger et al. 2023; Vasylyev et al. 2023). Several groups analyzed pre-explosion observations the SN site from the Hubble Space Telescope and the Large Binocular Telescope in the optical, and the Spitzer Space Telescope in the infrared. In all, these works find a putative progenitor object at the SN location whose spectral energy distribution is compatible with it being a dust-enshrouded RSG star. However, estimates of the zero-age main sequence (ZAMS) progenitor mass differed widely, from $M_{\text{ZAMS}} \approx 8 M_{\odot}$ to $M_{\text{ZAMS}} \approx 18 M_{\odot}$ (Qin et al. 2023, $18.1^{+0.7}_{-1.2} M_{\odot}$; Van Dyk et al. 2023, $12 - 15 M_{\odot}$; Kilpatrick et al. 2023, $11 \pm 2 M_{\odot}$; Jencson et al. 2023, $17 \pm 4 M_{\odot}$; Xiang et al. 2024, $12^{+2}_{-1} M_{\odot}$; Neustadt et al. 2024, $9 - 14 M_{\odot}$). Additional analyses of the stellar populations in the vicinity of the SN provided estimates of $M_{\text{ZAMS}} = 17 - 19 M_{\odot}$ (Niu et al. 2023), and $M_{\text{ZAMS}} \approx 22 M_{\odot}$ (Liu et al. 2023). A progenitor mass of $M_{\text{ZAMS}} = 20 \pm 4 M_{\odot}$ was found by So-raisam et al. (2023) by interpreting the observed variability of the pre-SN source in the IR observations as due to pulsational instability of an M-type star. Independently of the pre-explosion observations, Bersten et al. (2024) performed a hydrodynamical modelling of the bolometric light curve and photospheric velocity evolution and were able to constrain the progenitor mass to $M_{\text{ZAMS}} < 15 M_{\odot}$.

In this work, we present the first nebular spectrum of SN 2023ixf as an additional attempt to constrain the progenitor mass using independent information. The spectrum also serves to provide some insights on the internal structure of the SN ejecta through line profile analysis. Section 2 provides a description of the observational data. In Section 3 we analyze the nebular spectrum properties and we estimate a progenitor mass in Section 4. Our conclusions are summarized in Section 5.

2. Observations, reddening and distance

The spectrum presented in this work was obtained with the Gemini Multi-Object Spectrograph (GMOS; Hook et al. 2004) mounted on the Gemini North Telescope (Program GN-2024A-Q-139, PI Andrews). The observations were divided into four 900-s exposures in long-slit mode with the R400 grating. The data were processed with standard procedures using the IRAF Gemini package. Flux calibration was performed with a baseline standard observation. The spectrum resolution is $\approx 10 \text{ \AA}$ ($\approx 500 \text{ km s}^{-1}$ at 6000 \AA). Adopting the explosion time at $\text{JD} = 2460083.25$ (Hosseinzadeh et al. 2023), the spectrum phase is 259 days after the explosion.

The redshift published in the NASA/IPAC Extragalactic Database¹ (NED) for the host galaxy and used in this work is 0.0008. We additionally adopt a distance to M101 of $6.85 \pm 0.15 \text{ Mpc}$ (Riess et al. 2022), and a Milky-Way reddening of $E(B - V)_{\text{MW}} = 0.008 \text{ mag}$ (Schlafly & Finkbeiner 2011). Reddening in the host galaxy was estimated by Lundquist et al. (2023) to be $E(B - V)_{\text{Host}} = 0.031 \text{ mag}$. We applied the extinction correction by using a standard extinction law (Cardelli et al. 1989) with $R_V = 3.1$ and thus the total $E(B - V)_{\text{Total}} = 0.039 \text{ mag}$.

3. Spectral properties

The nebular spectrum of SN 2023ixf is presented in Figure 1, in comparison with two prototypical Type IIP SNe, SN 1999em at 230 d (Leonard et al. 2002) and SN 2004et at 253 d (Sahu et al. 2006). Typical spectral features of SNe II at this phase

are seen in the spectrum, most prominently the emissions from $\text{H}\alpha$, $[\text{O I}]\lambda\lambda 6300, 6364$, and $[\text{Ca II}]\lambda\lambda 7291, 7324$. Also identifiable are emission lines due to $\text{Mg I}\lambda 4571$ and the Ca IR triplet ($\text{Ca II}\lambda\lambda 8498, 8542, 8662$), and the P-Cygni profile due to the Na I D doublet ($\text{Na I}\lambda\lambda 5890, 5895$). No emission line is identifiable as $\text{H}\beta$. The $[\text{O I}]$ feature appears stronger relative to $\text{H}\alpha$ and the $[\text{Ca II}]$ doublet as compared with SN 1999em and SN 2004et (see more on this in Section 4). Except for the $[\text{Ca II}]$ doublet, the most prominent lines appear more blueshifted in SN 2023ixf than in its counterparts.

After comparing with the sample of Type II-P SNe from Silverman et al. (2017), we find that the emission lines appear in general broader in SN 2023ixf than in the other objects, except for SN 1992ad and SN 1993K. This is especially true in the case of $\text{H}\alpha$, which in SN 2023ixf shows a complex profile. More on this will be discussed in Sections 3.1 and 3.2.

3.1. Line profiles

As shown in Figure 1, most emission lines appear blueshifted in SN 2023ixf, except for $[\text{Ca II}]\lambda\lambda 7291, 7324$ that is centered nearly at rest. The line profiles of the main spectral features are shown in detail in Figure 2. In the case of $\text{H}\alpha$ the profile can be decomposed into two components, a wide one (with $\text{FWHM} = 5300 \text{ km s}^{-1}$) centered at rest, plus an intermediate-width one ($\text{FWHM} = 1600 \text{ km s}^{-1}$) shifted by -1800 km s^{-1} .

The $[\text{O I}]\lambda\lambda 6300, 6364$ feature exhibits the double-peak profile that is typically seen in nebular spectra of core-collapse SNe (Maeda et al. 2008; Modjaz et al. 2008; Taubenberger et al. 2009). The peaks are displaced roughly symmetrically relative to 6300 \AA . Both emission peaks appear to have complex profiles that can be decomposed into a wider ($\text{FWHM} \approx 2000 \text{ km s}^{-1}$) and a narrower ($\text{FWHM} \approx 500 \text{ km s}^{-1}$) component, as shown in Figure 3. The centers of the wider components are separated by $\approx 2500 \text{ km s}^{-1}$, at -1100 km s^{-1} and 1400 km s^{-1} , respectively. The narrower peaks are slightly further apart with a separation of $\approx 3000 \text{ km s}^{-1}$, and both peaks shifted by -1700 km s^{-1} and 1300 km s^{-1} , respectively. We note that such a separation of $\approx 3000 \text{ km s}^{-1}$ is roughly equal to that between the $[\text{O I}]\lambda 6300$ and $[\text{O I}]\lambda 6364$ lines that produce this feature. Similar blueshifts in $[\text{O I}]$ and $\text{H}\alpha$ were observed in SN 2007it (Andrews et al. 2011). Furthermore, a multiple-component feature in $[\text{O I}]$ has been seen before in SN 2016gkg, and has been attributed to multiple distinct kinematic components of material at low and high velocities (Kuncarayakti et al. 2020). Hypotheses on the material distribution in SN 2023ixf are discussed in Section 3.2.

In order to fit the four components that we attribute to $[\text{O I}]\lambda\lambda 6300, 6364$, we subtracted an additional set of wide and narrow Gaussian profiles centered at 6413 \AA (see Figure 3, left panel). This feature may also be present in the spectrum of SN 1999em (see Figure 1), and it may be attributed to $\text{O I}\lambda 6456$ blueshifted by $\approx 2000 \text{ km s}^{-1}$. However, this identification is not clear as the profile may be affected by a remainder absorption component of the $\text{H}\alpha$ line to the red. There is no clear explanation that could account for this permitted line. Furthermore, we do not recognize this feature in the sample of nebular spectra from Silverman et al. (2017).

Two emission features appear that may be identified as $[\text{O I}]\lambda 5577$ and $\text{O I}\lambda 7774$, although with a blueshift of 1500 km s^{-1} . This is shown in Figure 2, central panel. If the identifi-

² The width of these narrower lines is near the spectral resolution achieved by the data, so it may be considered as an upper limit to the actual width.

¹ <https://ned.ipac.caltech.edu/>

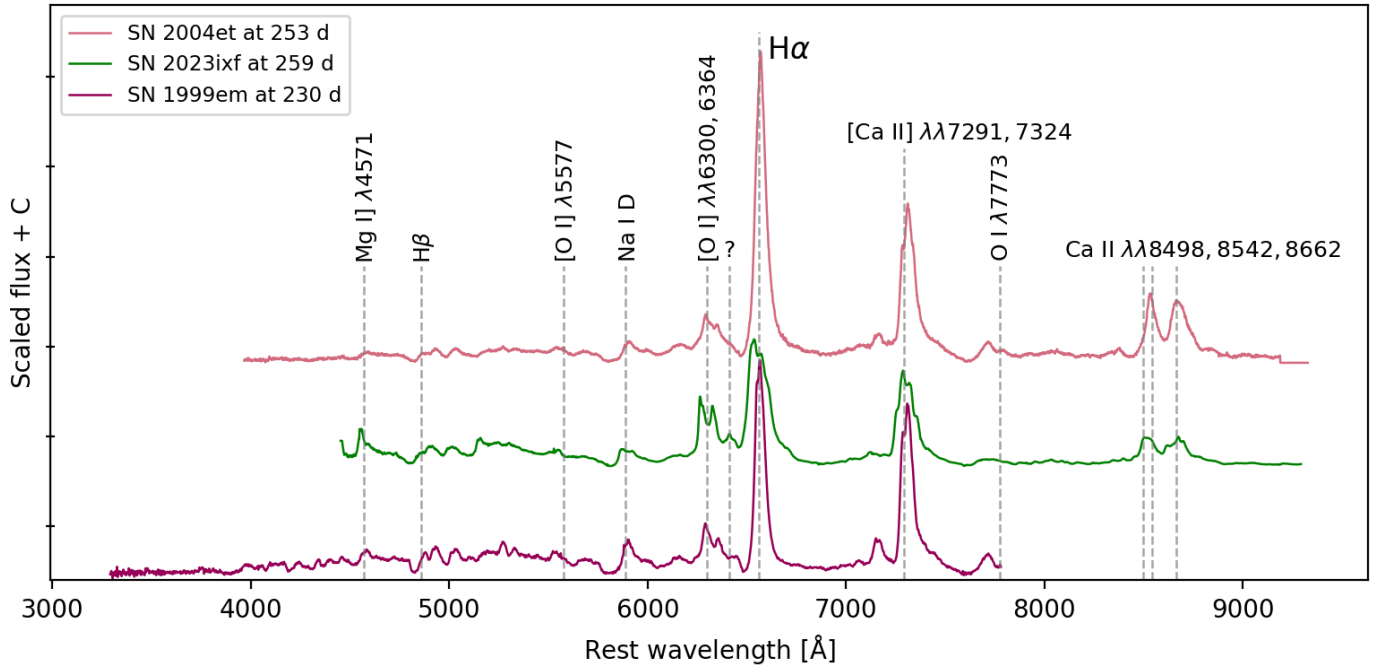


Fig. 1. Nebular spectra of SN 2023ixf compared with those of SN 1999em (Leonard et al. 2002) and SN 2004et (Sahu et al. 2006) at similar phases. The spectra are corrected for redshift and not extinction. Prominent emission features are indicated with gray vertical lines.

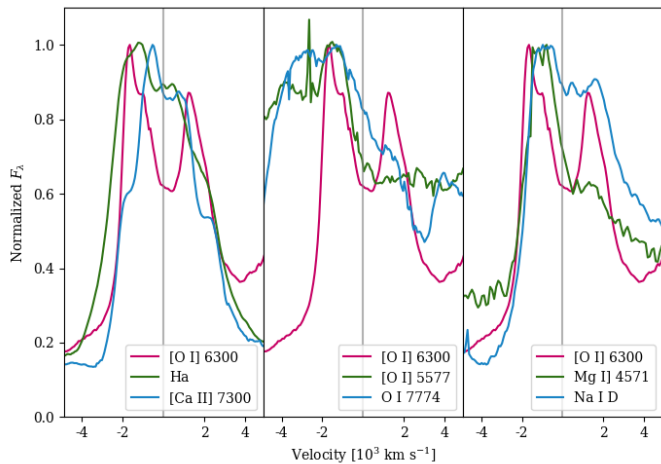


Fig. 2. Line profiles of several emission lines in 2023ixf.

cations are correct, the blueshifts are similar to those of the [O I] $\lambda\lambda 6300, 6364$ lines. Mg I] $\lambda 4571$ and Na I D are clearly identifiable in the spectrum, both blue-shifted by ≈ 1000 km s $^{-1}$, roughly similar to the other lines. Na I D shows a broad profile and an absorption produced by the interstellar medium (ISM) on top.

3.2. Ejecta geometry

The [O I] double-peaked profile described above is an indicator of an asymmetry in the ejecta (Kuncarayakti et al. 2020; Fang et al. 2022). It is also noticeable that the [Ca II] doublet is centered at rest wavelength. Thus, the disposition of the inner material could match that proposed by Fang et al. (2024), in which an axisymmetric oxygen-rich torus surrounds a bipolar calcium region (see their Figure 3). The general blueshift common to all

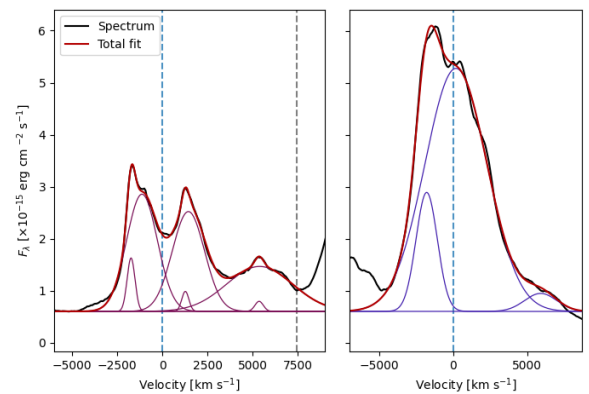


Fig. 3. Fitting of the [O I] doublet and H α profiles. Blue dashed lines indicate the rest wavelength for 6300 Å and 6564 Å in the left and right panels respectively, and the grey dashed line indicates the rest wavelength for 6456 Å. The thin lines show the individual gaussian components.

species supports this hypothesis, meaning that we may be mostly seeing the torus's near side while the far side is mostly obscured. In addition to this, an outer, roughly spherical, high-velocity H-rich material must be responsible for the wide, rest-centered H α component. Nevertheless, the two global, intrinsically different emitting regions of the ejecta, associated with the low- and high-velocities, may be challenging to explain in the context of the mechanism of the explosion, which takes place deep in the core. Here we highlight that the double-component (broad + narrow) line profile possibly occurs in all ejecta layers, from the outermost parts (H) down to the inner layers (O, Na, Mg) and core (Ca).

Another hypothesis that may explain these peculiar line profiles is the presence of an asymmetric or clumpy CSM that slows

down parts of the ejecta and thus produces narrow, blue-shifted line components. Moreover, the presence of CSM surrounding the SN has already been proposed for SN 2023ixf (e.g. [Bostroem et al. 2023](#); [Jacobson-Galán et al. 2023](#); [Martinez et al. 2024](#)). The extended, H-rich envelope is mainly unaffected and seen as a rest-centered profile, while a small part of the hydrogen and the regions rich in other elements are mostly affected by the CSM slow-down.

4. Progenitor mass

Nebular SN spectra are useful indicators of the progenitor mass. The flux of the [O I] $\lambda\lambda 6300, 6364$ feature has been proposed as an indicator of CO core mass by proxy of the O mass in the core ([Uomoto 1986](#); [Jerkstrand et al. 2014](#)). Given that absolute fluxes can be affected by errors in the spectral calibration or in the distance and extinction estimations, the flux ratios of [O I] $\lambda\lambda 6300, 6364$ over [Ca II] $\lambda\lambda 7291, 7324$ have been proposed as more robust indicators of the progenitor mass ([Fransson & Chevalier 1989](#); [Fang et al. 2022](#)). The relation between the [O I]/[Ca II] flux ratio and the progenitor ZAMS mass is seen in the model nebular spectra by [Jerkstrand et al. \(2014\)](#). Here we will derive a progenitor mass estimate by means of line fluxes and flux ratios, and by direct comparison with available model spectra.

In Figure 4 we show the 259 d spectrum of SN 2023ixf and modeled spectra computed by [Jerkstrand et al. \(2014\)](#) for SNe II at a similar age and for varying progenitor masses. The model spectra were scaled to match the distance to SN 2023ixf. A scaling factor of 1.15 was applied to the observed spectrum in order to match the synthetic VRI magnitudes with the observed ones available from the American Association of Variable Star Observers (AAVSO³) International Database. The value was calculated by taking an average of the scaling factor for each filter. From the Figure, it can be seen that the observed spectrum has suppressed emission of permitted lines from H α and Ca II IR triplet as compared with all of the modeled spectra. Nevertheless, if one compares the emissions due to [O I] and [Ca II], the modeled spectra from 12 and 15 M_{\odot} progenitors provide the closest matches to the observations.

In terms of the [O I]/[Ca II] flux ratio the value obtained from the observed spectrum is 0.51. Compared with ratios of 0.35, 0.60, 1.18, and 1.74 obtained from the modeled spectra with 12, 15, 19, and 25 M_{\odot} , respectively, the result is indicative of a ZAMS progenitor mass between 12 and 15 M_{\odot} . Furthermore, high-mass progenitors with $M_{\text{ZAMS}} \gtrsim 19 M_{\odot}$ are disfavored based on this comparison.

We also considered the nebular spectra models from [Dessart et al. \(2021\)](#) to double-check this result. Although the epochs differ in about 100 days, as the available models are calculated for 360 days post-explosion, the oxygen-to-calcium ratio does not show significant time variation in the spectra models from [Jerkstrand et al. \(2014\)](#). The measured ratio value for the SN 2023ixf is also consistent with progenitors with ZAMS mass below 15 M_{\odot} compared with measurements performed on the models from [Dessart et al. \(2021\)](#). The direct comparison also suggests a relatively low-mass progenitor, but we do not show it here as the nebular spectrum evolves significantly within 100 days. Further observations will enable us to use these models with more accuracy.

Another way of estimating the progenitor mass comes from the direct measurement of the [O I] doublet flux which constrains

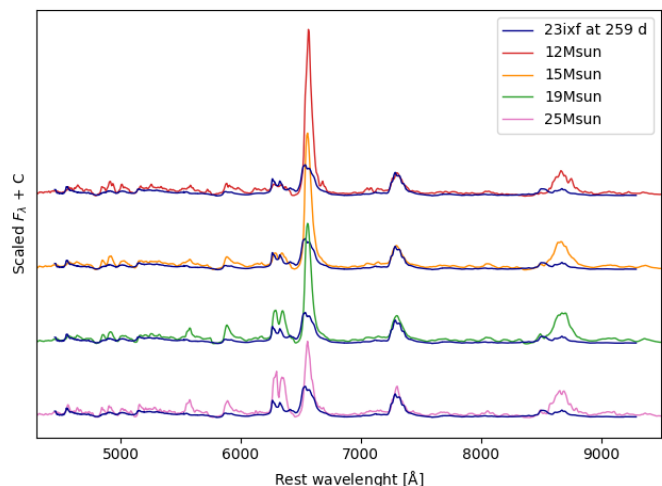


Fig. 4. SN 2023ixf at 259 d compared to nebular spectra models from [Jerkstrand et al. \(2014\)](#) at 250 d.

the minimum oxygen mass responsible for such emission. This mass is linked to the progenitor mass by theoretical oxygen production yields. This procedure is detailed in [Jerkstrand et al. \(2014\)](#) and has been used as an independent way of estimating the progenitor mass (e.g. [Sahu et al. 2011](#); [Kuncarayakti et al. 2015](#)). As mentioned before, the main uncertainties of this method lie in the absolute flux calibration (affected by the reddening correction and photometry scaling).

Assuming the emission with peak at 5550 \AA is [O I] $\lambda 5577$ blueshifted by $\approx 1500 \text{ km s}^{-1}$, we can establish a lower limit for the flux, as the continuum is not clear and the line might be blended with the [Fe I] $\lambda 5501$ line. Consequently, the lower limit for the material temperature is 3700 K ([Jerkstrand et al. 2014](#)). The oxygen doublet flux is $2.38 \times 10^{-13} \text{ erg s}^{-1} \text{ cm}^{-2}$, giving an oxygen mass of 0.5 M_{\odot} . We assume this is the total mass that produces the measured flux. According to the oxygen production yields published by [Nomoto et al. \(1997\)](#) and [Limongi & Chieffi \(2003\)](#), the progenitor must have been a star below 17 M_{\odot} . If we consider the production yields provided by [Rauscher et al. \(2002\)](#) and [Sukhbold et al. \(2016\)](#), the progenitor mass is well below 15 M_{\odot} . Because of the uncertainties involved in this last method (in the absolute flux calibration and the temperature determination, see [Jerkstrand 2017](#)), we prefer the former approach based on direct model comparison and flux ratios to constrain the progenitor mass. We thus conclude that the progenitor must have been a star with ZAMS mass between 12 and 15 M_{\odot} .

5. Conclusions

We present the first nebular spectrum of SN 2023ixf published in the literature, taken 259 days after the explosion. The observations were obtained with the Gemini North Telescope using GMOS. The spectrum was useful to examine the inner regions of the ejecta through line profiles and to determine the progenitor mass following a procedure independent from those previously published for this SN.

The spectrum shows the typical emission lines seen in a Type II SN resulting from the elements hydrogen, oxygen, calcium, sodium, and magnesium. In comparison with other Type II SNe, SN 2023ixf presents a weaker H α emission, and no H β is recognizable. The [O I] doublet is blue-shifted and shows a double-peaked profile. This is a sign of a non-spherical ejecta and may

³ <https://www.aavso.org>

be interpreted as a torus-shaped emitting region. By fitting the line we distinguish two wide components and two narrow components, also distinguishable as intermediate line peaks in the $H\alpha$ profile, and other lines as well. This feature, also detected in Mg I]44571 and Na I D, is attributed to a low-velocity ejecta component, caused either by two distinct ejecta regions or by parts of the material being partly slowed down by an asymmetric or clumpy CSM. $H\alpha$ wide component is rest-centered and must be produced by an outer, roughly spherical, H-rich material.

The main result of our work is the estimation of the progenitor mass from the nebular spectrum. Via spectral comparison with models by Jerkstrand et al. (2014) we found that the progenitor mass was between 12 and 15 M_{\odot} . This was confirmed by comparing the [O I]/[Ca II] flux ratio between the spectrum of SN 2023ixf and those of the models. We also derived an upper limit of 15 – 17 M_{\odot} for the progenitor mass based on the [O I] flux. However, this result is less constraining and less reliable than the comparison with model spectra. Our derived mass is in agreement with the estimates of Bersten et al. (2024) from hydrodynamical modelling and also Kilpatrick et al. (2023); Xiang et al. (2024); Van Dyk et al. (2023) and Neustadt et al. (2024) from pre-explosion images.

Acknowledgements. We thank Dave Sand and Jeniveve Pearson, CoI's for the Gemini Program GN-2024A-Q-139, for sharing the observational data. We thank the Gemini Observatory for encouraging fluid group interaction between Programs GN-2024A-Q-139 and GN-2024A-Q-309 teams. H.K. was funded by the Research Council of Finland projects 324504, 328898, and 353019. We acknowledge with thanks the variable star observations from the AAVSO International Database contributed by observers worldwide and used in this research. Based on observations obtained at the international Gemini Observatory (GN-2024A-Q-139, PI: Andrews), a program of NSF's NOIRLab, which is managed by the Association of Universities for Research in Astronomy (AURA) under a cooperative agreement with the National Science Foundation. On behalf of the Gemini Observatory partnership: the National Science Foundation (United States), National Research Council (Canada), Agencia Nacional de Investigación y Desarrollo (Chile), Ministerio de Ciencia, Tecnología e Innovación (Argentina), Ministério da Ciência, Tecnologia, Inovações e Comunicações (Brazil), and Korea Astronomy and Space Science Institute (Republic of Korea). This work was enabled by observations made from the Gemini North telescope, located within the Maunakea Science Reserve and adjacent to the summit of Maunakea. We are grateful for the privilege of observing the Universe from a place that is unique in both its astronomical quality and its cultural significance.

References

Andrews, J. E., Sugerman, B. E. K., Clayton, G. C., et al. 2011, *ApJ*, 731, 47
 Berger, E., Keating, G. K., Margutti, R., et al. 2023, *ApJ*, 951, L31
 Bersten, M. C., Orellana, M., Folatelli, G., et al. 2024, *A&A*, 681, L18
 Bostroem, K. A., Pearson, J., Shrestha, M., et al. 2023, *ApJ*, 956, L5
 Cardelli, J. A., Clayton, G. C., & Mathis, J. S. 1989, *ApJ*, 345, 245
 Davies, B. & Beasor, E. R. 2018, *MNRAS*, 474, 2116
 Dessart, L., Hillier, D. J., Sukhbold, T., Woosley, S. E., & Janka, H. T. 2021, *A&A*, 652, A64
 Fang, Q., Maeda, K., Kuncarayakti, H., & Nagao, T. 2024, *Nature Astronomy*, 8, 111
 Fang, Q., Maeda, K., Kuncarayakti, H., et al. 2022, *ApJ*, 928, 151
 Fransson, C. & Chevalier, R. A. 1989, *ApJ*, 343, 323
 Grefenstette, B. W., Brightman, M., Earnshaw, H. P., Harrison, F. A., & Margutti, R. 2023, *ApJ*, 952, L3
 Hiramatsu, D., Tsuna, D., Berger, E., et al. 2023, *ApJ*, 955, L8
 Hook, I. M., Jørgensen, I., Allington-Smith, J. R., et al. 2004, *PASP*, 116, 425
 Hosseinzadeh, G., Farah, J., Shrestha, M., et al. 2023, *ApJ*, 953, L16
 Jacobson-Galán, W. V., Dessart, L., Margutti, R., et al. 2023, *ApJ*, 954, L42
 Jenson, J. E., Pearson, J., Beasor, E. R., et al. 2023, *ApJ*, 952, L30
 Jerkstrand, A. 2017, in *Handbook of Supernovae*, ed. A. W. Alsabti & P. Murdin, 795
 Jerkstrand, A., Fransson, C., Maguire, K., et al. 2012, *A&A*, 546, A28
 Jerkstrand, A., Smartt, S. J., Fraser, M., et al. 2014, *MNRAS*, 439, 3694
 Kilpatrick, C. D., Foley, R. J., Jacobson-Galán, W. V., et al. 2023, *ApJ*, 952, L23
 Kuncarayakti, H., Folatelli, G., Maeda, K., et al. 2020, *ApJ*, 902, 139
 Kuncarayakti, H., Maeda, K., Bersten, M. C., et al. 2015, *A&A*, 579, A95

Leonard, D. C., Filippenko, A. V., Gates, E. L., et al. 2002, *PASP*, 114, 35
 Limongi, M. & Chieffi, A. 2003, *ApJ*, 592, 404
 Liu, C., Chen, X., Er, X., et al. 2023, *ApJ*, 958, L37
 Lundquist, M., O'Meara, J., & Walawender, J. 2023, *Transient Name Server AstroNote*, 160, 1
 Maeda, K., Kawabata, K., Mazzali, P. A., et al. 2008, *Science*, 319, 1220
 Martinez, L., Bersten, M. C., Folatelli, G., Orellana, M., & Ertini, K. 2023, *arXiv e-prints*, arXiv:2310.08733
 Martinez, L., Bersten, M. C., Folatelli, G., Orellana, M., & Ertini, K. 2024, *A&A*, 683, A154
 Maund, J. R., Smartt, S. J., & Danziger, I. J. 2005, *MNRAS*, 364, L33
 Modjaz, M., Kirshner, R. P., Blondin, S., Challis, P., & Matheson, T. 2008, *ApJ*, 687, L9
 Neustadt, J. M. M., Kochanek, C. S., & Smith, M. R. 2024, *MNRAS*, 527, 5366
 Niu, Z., Sun, N.-C., Maund, J. R., et al. 2023, *ApJ*, 955, L15
 Nomoto, K., Hashimoto, M., Tsujimoto, T., et al. 1997, *Nucl. Phys. A*, 616, 79
 Perley, D. A., Gal-Yam, A., Irani, I., & Zimmerman, E. 2023, *Transient Name Server AstroNote*, 119, 1
 Qin, Y.-J., Zhang, K., Bloom, J., et al. 2023, *arXiv e-prints*, arXiv:2309.10022
 Rauscher, T., Heger, A., Hoffman, R. D., & Woosley, S. E. 2002, *ApJ*, 576, 323
 Riess, A. G., Yuan, W., Macri, L. M., et al. 2022, *ApJ*, 934, L7
 Sahu, D. K., Anupama, G. C., Sridivya, S., & Muneer, S. 2006, *MNRAS*, 372, 1315
 Sahu, D. K., Gurugubelli, U. K., Anupama, G. C., & Nomoto, K. 2011, *MNRAS*, 413, 2583
 Schlafly, E. F. & Finkbeiner, D. P. 2011, *ApJ*, 737, 103
 Silverman, J. M., Pickett, S., Wheeler, J. C., et al. 2017, *MNRAS*, 467, 369
 Smartt, S. J. 2015, *PASA*, 32, e016
 Smith, N., Pearson, J., Sand, D. J., et al. 2023, *ApJ*, 956, 46
 Soraisam, M. D., Szalai, T., Van Dyk, S. D., et al. 2023, *ApJ*, 957, 64
 Sukhbold, T., Ertl, T., Woosley, S. E., Brown, J. M., & Janka, H. T. 2016, *ApJ*, 821, 38
 Taubenberger, S., Valenti, S., Benetti, S., et al. 2009, *MNRAS*, 397, 677
 Teja, R. S., Singh, A., Basu, J., et al. 2023, *ApJ*, 954, L12
 Uomoto, A. 1986, *ApJ*, 310, L35
 Van Dyk, S. D., Cenko, S. B., Poznanski, D., et al. 2012, *ApJ*, 756, 131
 Van Dyk, S. D., Srinivasan, S., Andrews, J. E., et al. 2023, *arXiv e-prints*, arXiv:2308.14844
 Vasylyev, S. S., Yang, Y., Filippenko, A. V., et al. 2023, *ApJ*, 955, L37
 Xiang, D., Mo, J., Wang, L., et al. 2024, *Science China Physics, Mechanics, and Astronomy*, 67, 219514